

Received January 4, 2017, accepted January 24, 2017, date of publication February 6, 2017, date of current version March 13, 2017.

Digital Object Identifier 10.1109/ACCESS.2017.2664580

Modeling and Implementation of Electroactive Smart Air-Conditioning Vent Register for Personalized HVAC Systems

JINLONG YAN^{1,2}, QI ZENG³, YUAN LIANG², LEI HE², AND ZHENGPING LI¹

¹School of Electronic and Information Engineering, Anhui University, Hefei 230601, China

²Department of Electrical Engineering, University of California at Los Angeles, Los Angeles, CA 90095, USA

³Department of Electrical Engineering, Tsinghua University, Beijing 100084, China

Corresponding author: Z. Li (bluefeynman@outlook.com)

This work was supported in part by the National Natural Science Foundation of China under Grant 61474001 and in part by the China Scholarship Council under Grant 201506500001.

ABSTRACT This paper presents a novel heating, ventilation, and air-conditioning system that can achieve significant energy savings. A smart register that can reduce overall energy costs by up to 30%, compared to conventional devices, is demonstrated. A high abstraction model based on a computational fluid dynamics (CFD) simulation is developed to predict the diffused airflow from the register. The model is validated to within a 10% error, and is found to be 1000 times more efficient than the detailed CFD simulations. Finally, a prototype of the electroactive smart air-conditioning vent register is implemented, and adjustments of the register's tunnels are implemented.

INDEX TERMS Circuit optimization, energy efficiency, modeling, embedded software, energy saving, personalized HVAC system.

I. INTRODUCTION

The energy crisis and the problem of carbon emissions have become two serious concerns in recent decades. The energy Internet (EI) has aroused global attention as one possible solution [1]. Furthermore, big-data applications in a smart-grid scenario can attain a significant effect. According to the Energy Information Administration (EIA), heating, ventilation, and air-conditioning (HVAC) in buildings accounts for about 13% of the total energy consumption in the United States [1]. In addition to big-data applications in a smart-grid scenario [2] the reduction of energy losses that arise when power flows from one bus to another in a smart grid [3], as well as the reduction of energy consumption and the cost of HVAC has become a major target for curbing electricity usage and reducing greenhouse gas emissions. Great efforts are being put into improving HVAC efficiency. When the cost of retrofitting is considered, the implementation of new control and sensing layers is clearly preferable to the replacement of an entire HVAC system [5].

One approach to realizing the optimal control of HVAC is the use of personalized ventilation (PV) [6], whereby conditioned air is delivered directly to indoor spaces.

Yang *et al.* [7], [8] proposed a system combining PV devices with mixing ventilation systems based on personal ceiling-mounted nozzles. This design permits the easy extension of existing HVAC systems and was reported as realizing a 5% energy saving over a conventional arrangement. Lo *et al.* [9] reported on a PV system with inner looping airflow patterns, which uses multiple slot diffusers to provide angled jets of air and a central return vent to limit the air movement. Their energy simulation results showed approximately 12% savings in the total cooling energy. Makhoul *et al.* [10] developed a coaxial personal ventilation nozzle with a primary fresh air nozzle with integrated peripheral diffusers. The nozzle uses a high-velocity jet to bring fresh air to the breathing level. Their system achieved improved air quality at the occupant's location and showed a 1.97°C thermal localization, according to the simulation, which indicates an energy saving of 28% in some cases.

However, existing PV systems face several challenges that prevent their large-scale deployment. First, because of their reliance on conventional airflow patterns from the vents, there are limited room temperature set-point extensions shown in the thermal distribution. This creates major difficulties when

attempting to introduce an effective zone-based control that divides the area in an open room without walls into thermal zones. In addition, most systems attain good energy-saving effects only when the occupants of the room are sedentary. There is currently no technique that combines the occupant locations and registers with active ventilation control.

This paper presents a PV system that employs new airflow patterns created using a newly designed smart register, and the corresponding control systems. The overall system design is described in Section II. The energy saving potential of the system is illustrated by comparisons with a conventional conditioning system, through case studies. We also show how the desired airflow patterns can be achieved using a smart register with funnel-shaped tunnels and how the airflow configurations can be modified by changing the geometry. In Section III, a mathematical model of the airflow through a register is built, to describe the flow patterns and enable subsequent wind speed conditioning optimization. We then present a prototype of the manufactured register, as well as the circuit design for sensing and activation, such that it functions as a closed loop.

II. CONCEPT OF eSaver SYSTEM

A. CONDITIONING WITH THERMAL ENVELOPE

The proposed PV system supplies conditioned air directly to the occupant, with acceptable thermal and wind comfort. It also achieves an enhanced temperature difference between the outside and inside of the thermal envelope around the occupant. Fig. 1 is a schematic of the proposed airflow patterns and the overall system implementation with the designed register and control circuits. The register is modeled with 3D printing and covered with BSEP material at the outlet, which is activated by a power supply to modify the air direction and volume. As illustrated, the airflow from a duct is modulated by a damper, and it passes through the register to enter a room, to directly cool or warm the occupants. The edge tubes are funnel shaped with smaller outlets to speed up the airflow and form an air curtain around the occupant, which serves two functions: (1) reducing the diffusion of low-speed conditioned air in the center without affecting the occupant's comfort, (2) creating a localized thermal environment without significantly conditioning the unoccupied area. The center airflow is jetted from the central funnel tubes with the larger outlets to slow down the air before it is jetted at the occupant, for reasons of better comfort.

To validate the feasibility and impact of the proposed conditioning scheme, we developed detailed 3D thermal models using Ansys Fluent to simulate the situation of one occupant in a typical office. The simulations were applied to the geometric model shown in Fig. 2. The model includes a thermal cylinder representing a standing person, located underneath the proposed register mounted in the ceiling. A constant temperature was applied to the human body to simulate the heat exchange between the body and the surroundings. There are two symmetrical return vents in the

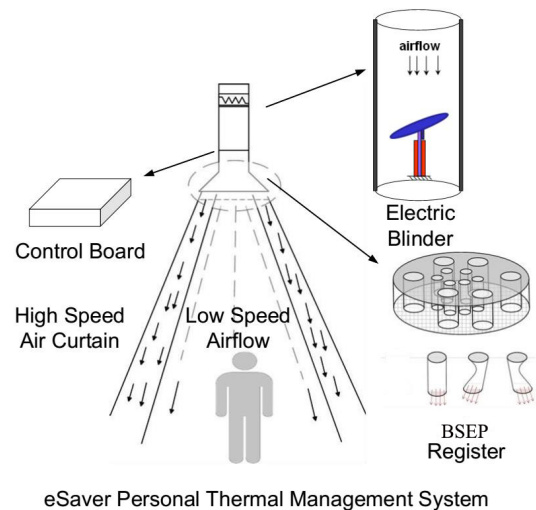


FIGURE 1. Overall system design of eSaver.

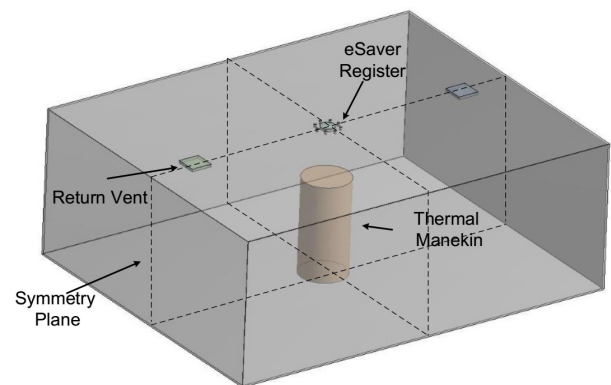


FIGURE 2. Geometry of simulation design.

ceiling, which are responsible for the recirculation of the air. A constant heat gain is maintained inside the room to simulate indoor thermal loads such as that produced by electrical equipment, as suggested in the ASHRAE standard [11]. In addition, various outer wall temperatures are applied to models simulating different outdoor thermal conditions, which constitute the major cooling and heating loads of the room. A summary of the important simulation settings are presented in Table 1.

We compare the temperature distributions in the rooms when using the eSaver and the conventional cooling method (Figs. 3(a), 4(a)). We can observe a large temperature difference between the outside and inside of the thermal envelope around the occupant. This shows that the eSaver can achieve an obvious thermal localization effect, which results in the isolation of the air curtain, implying considerable energy-saving potential. Moreover, we can see from the airflow velocity distribution (Figs. 3(b), 4(b)) that the average air speed around the occupant with the eSaver system is only slightly larger than that in a conventional system, which is within the occupant's comfort requirements. This is because, although the eSaver provides direct ventilation to the occupant, the center airflow is slowed by the register to avoid

TABLE 1. Important parameters used for room simulation setup.

Room			
Dimensions	7.82 m (L) × 6.1 m (W) × 2.5 m (H)	Indoor Thermal Load	72 W
Heat Transfer Coeff.	1.5 W/km ²	Humidity Range	30-60%
Occupant			
Height	1.83 m	Body Volume	1.145 m ³
Skin Temperature	93 °F	Surface Area	1.8 m ²
Environment			
Temperature (Cooling)	95 °F	Temperature (Heating)	42.8 °F

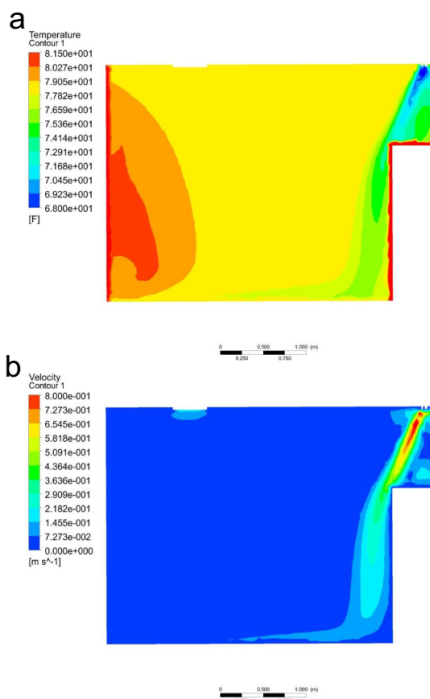


FIGURE 3. Temperature (a) and airflow velocity (b) distribution contour with eSaver conditioning from one half of symmetric intersection surface of the room.

over-exposure of the body to an air flow, and a higher-speed air curtain is used to reduce the center air diffusion.

We summarize several important indexes for evaluating the performance of the above cooling and heating scheme. It can be seen that the temperature at the occupant is between the desired 74.92°F and 77.53°F. The temperature of the occupant’s head is lower than that of the feet. The overall average air speed around the body is 0.181 m/s, which is within the range of the 10% predicted percentage of dissatisfaction. Thus, all the parameters satisfied the aforementioned ASHRAE standard [11]. Most importantly, the predicted set-point expansion, which is the horizontal temperature difference between the inside and outside of the air curtain is 4.32°F for cooling, and 10.08°F for heating, which is much larger than the value of 3.12°F mentioned in a previous work using a different PV method [10]. This guarantees the energy-saving potential of our system.

B. AIRFLOW REGULATION WITH DESIGNED REGISTER

The biggest challenge in implementing the described conditioning scheme is the obtaining of different airflow outlet

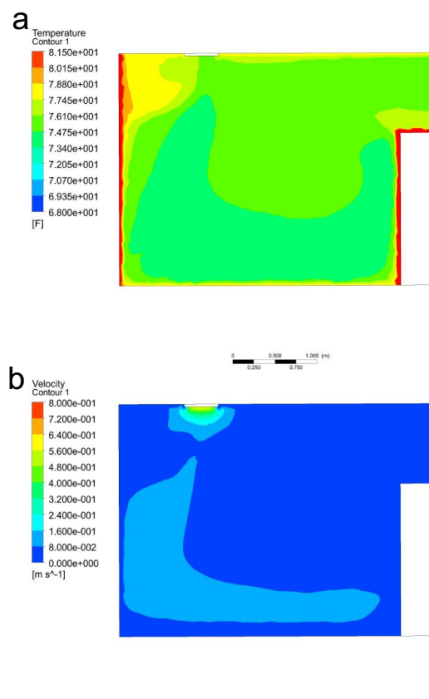


FIGURE 4. Temperature (a) and airflow velocity (b) distribution contour with conventional conditioning from one half of symmetric intersection surface of the room.

velocities from a range of tunnels. One obvious solution is to use an array of air jets, with different air sources, some emanating high-speed air to form an air curtain, and the rest emanating low-speed center air. However, this design is expensive to manufacture and is not compatible with existing HVAC ducts. Instead of using many jets, the eSaver takes advantage of the funnel effect, as shown in Fig. 5. The register contains two types of air jets—edge and central jets. The airflows from the ducts, all having the same velocity, are distributed through different tunnels in rough proportion to the opening sizes of the inlets in terms of volume. The edge jet has a funnel shape with a smaller outlet, which can accelerate the airflow to form an air curtain. The center jet is also funnel-shaped, but the outlet is larger than the inlet; thus, it slows down the airflow and improves the thermal comfort when directed at an occupant.

To validate the design’s ability to modulate the airflow, we demonstrate the airflow patterns of the previous cooling cases, as achieved using the designed register, by 3D computational fluid dynamics (CFD) simulations.

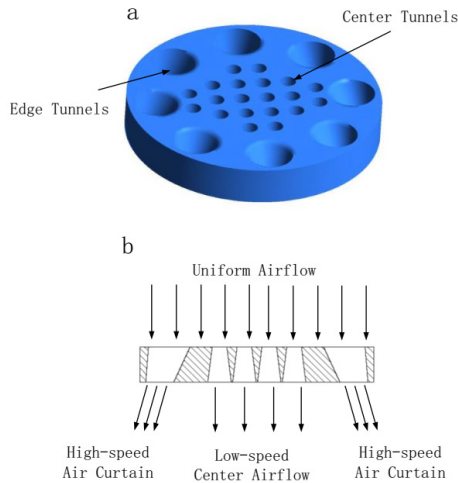


FIGURE 5. Working pattern of eSaver register: 3D view (a) and sectional view (b).

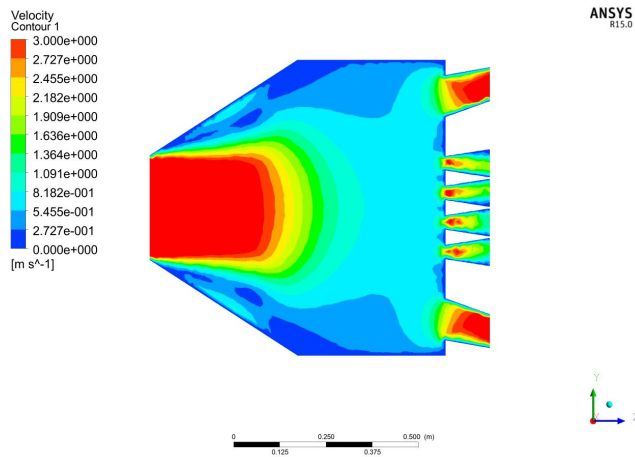


FIGURE 6. In-duct air distribution for cooling ventilation case.

TABLE 2. Important parameters used for register simulation.

Duct diameter	8 inch	Register thickness	3 inch
Max air speed	7 m/s	Min air speed	2 m/s
Cooling air temp.	68.0°F	Heating air temp.	85.0°F

The setup parameters for the simulation are listed in Table 2. The duct size and in-duct air volume conform to typical HVAC standard reference values, as indicated by ASHRAE [11]. The register’s geometries are shown in Fig. 5 and the dimensions are listed in Table 2.

For cooling applications, the designed register configuration produces the in-duct air distributions shown in Fig. 6. The in-duct air is first slowed down when it arrives at the register from the duct. It is then distributed to the edge and center tunnel inlets, where it is either slowed down or accelerated through the funnel-shaped tunnels to form the desired airflow patterns for heating or cooling, as mentioned in the previous section.

More detailed simulations have been carried out for registers with different tunnel configurations. We found that the

funnel-shaped tunnels are capable of slowing down or speeding up the airflow, depending on the tunnel sizes; therefore, the air flowing out of any one tube may be for the high-speed air curtain or the low-speed center air. Particularly, for the airflow in the duct, when the velocity is between 2.5 and 4 m/s, we could obtain an air curtain velocity of 2.986 to 2.013 m/s, and a center air velocity of 0.861 to 1.242 m/s.

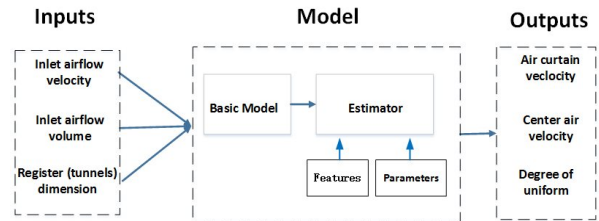


FIGURE 7. High abstraction model structure.

III. HIGH-ABSTRACTION MODEL OF AIRFLOW THROUGH REGISTER

In this section, we introduce a high abstraction model for predicting the air volume and velocity at the outlet of the register. With different tunnel shapes and inlet air volumes, the register can produce various airflow patterns for the center air and air curtain. The simulation of the airflow patterns, using current commercial CFD software, with the register models and boundary conditions given, is very time-consuming, and is not good enough for iteration-based register design optimization. Moreover, the simulated output is in three dimensions and produces an overwhelming amount of detailed fluid information that is not particularly helpful with the register design. Thus, we implemented a model that can provide abstracted information on the airflow and reduce the simulation time by a factor of 1000 by replacing the partial differential functions with empirical formulations. The structure of the model is shown in Fig. 7.

A. BASE MODEL

First, we constructed a basic model according to the principles of hydrodynamics, specifically, the mechanism of mass conservation. For this model, we assume that the inlet pressures for both the central tunnel and edge tunnels are equal. This gives:

$$V_{out_edge} = v_{in} \cdot S_{in} \cdot \frac{n_{edge} \cdot S_{out_edge}}{n_{edge} \cdot S_{out_edge} + n_{center} \cdot S_{out_center}}, \tag{1}$$

$$v_{out_edge} = \frac{V_{out_edge}}{n_{edge} \cdot S_{out_edge}}, \tag{2}$$

where v_{out_edge} represents the average velocity of airflow from the edge tunnels, which is given by the prediction; V_{out_edge} is defined as the amount of air. v_{in} and S_{in} denote the velocity and area, respectively, of the tube from the inlet; S_{out_edge} and S_{out_center} are defined as the sizes of the outlet areas for the edge and central tunnels, respectively. Here, n_{edge} and n_{center} are the number of small holes constituting the

edge and center outlets, respectively. This formulation helps us find the relationship between the original inlet and outlet velocities of the edge tunnels.

However, the airflow patterns at the outlet do not conform to the basic formulation, as the patterns can be affected by many factors including the inlet velocity and register dimensions. Moreover, it is much more difficult to construct a model for the airflow patterns at the central outlet. This is because the velocity distributions of the center airflows are much less uniform than those of the air curtain because of the shapes of the central tunnels.

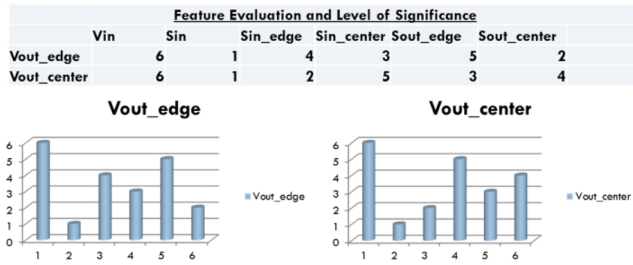


FIGURE 8. Feature evaluation.

B. FEATURE CONSTRUCTION AND SELECTION

Using the basic model, we constructed an estimator using the Buckingham Theorem [12] to more accurately describe the airflow patterns at the outlets. As many factors contribute to the physical processes, they should all be considered in our model. We selected features and chose the most important factors, to reduce the degree of complexity and coupling. Different feature selection methods have been developed such as the Relief [13], Filter [14], and Wrapper [15] methods. In this paper, we obtain a subset of important variables with rankings, which can be used as features in the model. The results are shown in Fig. 8.

We can see from the figure that, for the airflow velocities at the outlets of both the edge and central tunnels, the inlet airflow velocity has the greatest impact, which is very straightforward. We can also see that other factors have various degrees of impact when we compare the ranking results of the two variables, which means that we need to consider several factors affecting formulations during modeling.

C. MODEL FORMULATION

According to the rankings, we used the inlet velocity, inlet area, and outlet area of the edge/central duct as the most representative features, as they have the highest rankings and couple less.

TABLE 3. Errors of integrated model before and after estimation.

	Max error	RMSE
	after (before)	after (before)
Edge	10.23% (10.62%)	9.67% (9.99%)
Center_low	12.32% (15.72%)	3.95% (4.13%)
Center_high	36.41% (37.78%)	23.93% (24.43%)

Moreover, due to the assumptions of even distribution of pressure and flow of velocity in a single tunnel, errors are introduced into the model, which we need to take into consideration.

First, we construct features to fit the distribution of pressure, by utilizing the inlet velocity and inlet dimension information, which can be obtained from Eq. 4:

$$v'_{out_edge} = v_{out_edge} \cdot g_1(v_{in}), \quad (3)$$

$$g_1(v_{in}) = \alpha_1 \cdot v_{in} + \alpha_2, \quad (4)$$

where $\alpha_1 = -0.2217$, $\alpha_2 = 1.171$. Then, the airflow inside the tunnel is fitted using the inlet and outlet size information. We have:

$$v''_{out_edge} = v'_{out_edge} \cdot g_2\left(\frac{S_{out_edge}}{S_{in_edge}}\right), \quad (5)$$

$$g_2\left(\frac{S_{out_edge}}{S_{in_edge}}\right) = \alpha_3 \frac{S_{out_edge}}{S_{in_edge}} + \alpha_4, \quad (6)$$

where $\alpha_3 = 0.108$ and $\alpha_4 = 0.8988$. Finally, we achieve the relationship between the original inlet velocity and the outlet velocity of the edge tunnels, as above. The performance and errors in our model, for the edge tunnels, are shown in Table 3 (before estimation).

Now, we have the prototype of our model for the edge tunnels. The outlet airflow volume velocity can be calculated using Eq. 8 by utilizing the mass conservation of airflow volumes at the inlet and outlet.

$$V_{out_center} = v_{in} \cdot S_{in} - n_{edge} \cdot v_{out_edge} \cdot S_{out_edge}, \quad (7)$$

$$v_{out_center} = \frac{V_{out_center}}{n_{center} \cdot S_{out_center}}. \quad (8)$$

However, according to the simulation results, the center velocity is more complicated than the edge velocity, as the velocity is not uniformly distributed. The velocity distributions are shown in Fig. 6.

The uniform distribution of the center airflow is of vital importance to the performance of personal ventilation. Thus, we need a new parameter, the degree of uniformity (DoU),

$$v'_{out_edge} = (\alpha_1 \cdot v_{in} + \alpha_2) \cdot \left(\alpha_3 \frac{S_{out_edge}}{S_{in_edge}} + \alpha_4\right) \cdot v_{out_edge}, \quad (9)$$

$$v'_{out_center} = \begin{cases} (\beta_1 \cdot v_{out_center} + \beta_2), & v_{in} < 0.5m/s \\ \left(\beta_1 \frac{S_{in_center}}{S_{out_center}} + \beta_2\right) \cdot (1000\beta_3 \cdot S_{in_center} + \beta_4) \cdot v_{out_center}, & v_{in} < 0.5m/s. \end{cases} \quad (10)$$

to characterize the velocity distribution of the airflow from the center outlet. DoU is defined as the ratio of maximum velocity of the airflow to the average value, and can be fitted using a piece-wise model based on the inlet velocity of the register. The piece-wise model is formulated as shown in Eq. 9, as shown at the bottom of the previous page.

At this point, we have reached a high abstraction model for predicting the airflow patterns of the center air and the air curtain when the register dimensions and inlet airflows are given. The performance of the model is described in Table 3 (before estimation).

We can see that the root mean square error (RMSE) for the edge tunnel and central tunnel at low speeds is quite good, and that the value for the high-speed case of the central tunnel is relatively high. When we considered the data sets that produced the maximum errors, we found that this might be partially caused by the convergence of the simulation.

TABLE 4. New parameters sets.

	α_1	α_2	α_3	α_4
Edge	0.163656	-1.149604	-0.125394	-0.852910
Center low	-2.83300	2.321638	0	0
Center high	-2.673104	2.587613	0.120300	0.598667

D. PARAMETER ESTIMATION AND MODEL VALIDATION

Note that all the parameters in the model are obtained separately by minimizing the residual errors in the model, in order of their significance. Thus, only the local optimization of the parameters is granted. To further improve the prediction ability, we performed a second estimate with all the parameters optimized. [17]. The new parameters are listed in Table 4. The performance and errors of our integrated model are listed in Table 3 (after estimation).

To conclude, the entire model is formulated as per Eqs. 9 and 10, as shown at the bottom of the previous page. where,

$$v_{out_edge} = \frac{V_{out_edge}}{n_{edge} \cdot S_{out_edge}}$$

$$V_{out_edge} = \frac{v_{in} \cdot S_{in} \cdot n_{edge} \cdot S_{out_edge}}{n_{edge} \cdot S_{out_edge} + n_{center} \cdot S_{out_center}}$$

$$v_{out_center} = \frac{V_{out_center}}{n_{center} \cdot S_{out_center}},$$

$$V_{out_center} = v_{in} \cdot S_{in} - V_{out_edge}.$$

IV. PROTOTYPE OF eSaver

A. OVERALL DESIGN

This section describes the design of a register covered with a polymer material, and explains the reasons why this design can achieve tunnel changes. Then we describe the design of the actuating system that can control the tunnels in real time.

1) MATERIAL ATTACHMENT

The smart register consists of two parts—the stationary funnel-shaped tunnels and an innovative electro-active

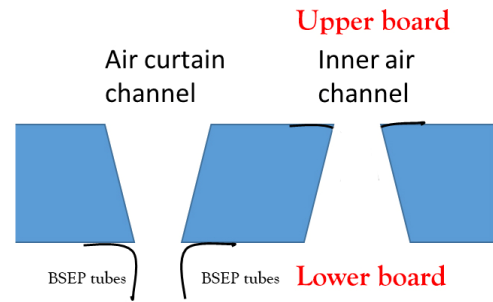


FIGURE 9. Method of attaching BSEP material.

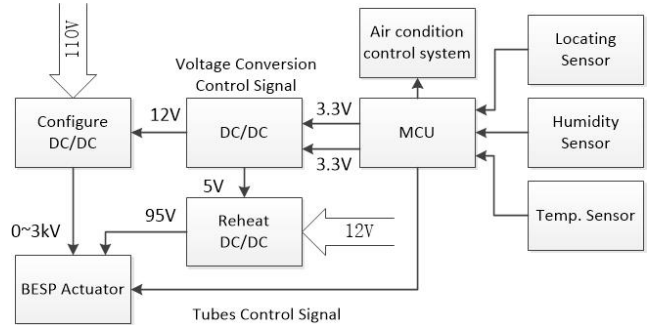


FIGURE 10. Hardware and voltages.

polymer (EAP) attached, as shown in Fig. 9. The funnel tunnels can achieve different air speeds, creating both an air curtain to achieve localized cooling/heating as well as a slow airflow in the central areas to improve comfort. Many kinds of EAPs have been developed, which are capable of electrically induced large-strain deformations [18], [19]. We try to use one type of EAP—a bistable EAP (BSEP) [20]—in the tubes to change the direction of the air. One side of the material is attached to the air outlet, while the material can be changed to bend at different angles using a control voltage. The tubes can be actuated to assume different angles (60° to 120°), and each tube can be individually controlled in real time. The airflow can be adjusted to cover an entire room and to follow an occupant moving at 1 m/s.

2) WORKING LOGISTICS

The overall hardware system is designed as shown below (Fig. 10). We use the original HVAC control system to check the indoor temperature and control whether cooling or heating is required. In addition, a location sensor is used to detect occupant movement. These data are used to control the voltage converter that produces the correct voltage to drive the BSEP tubes. The BSEP tubes are actuated to change the localized cooling/heating areas to follow the moving occupant.

Based on the hardware system and the characteristics of the material (Fig. 11), we designed a software control system for the eSaver register. The software design flow is shown below (Fig. 12). After initialization, the detection system continuously monitors whether a person is present in the corresponding area or not. If a person is detected, the system will check the current tube directions. If they conform to

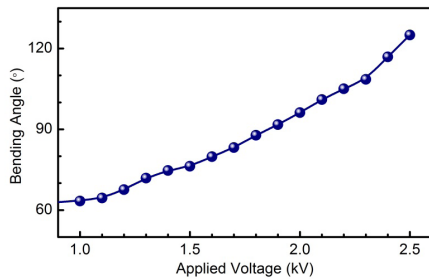


FIGURE 11. Material-bending characteristics.

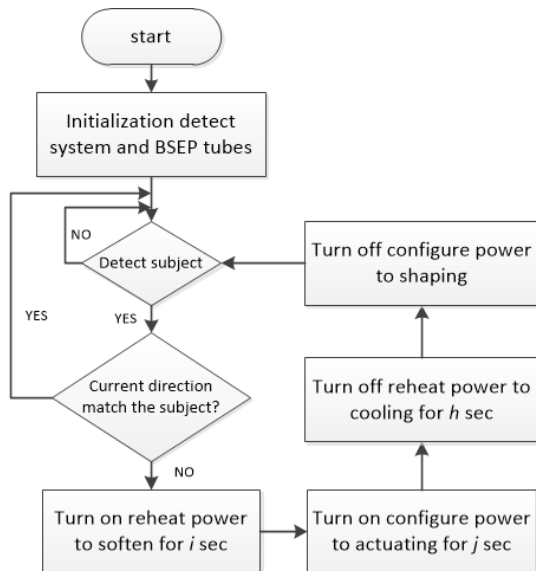


FIGURE 12. Software workflow.

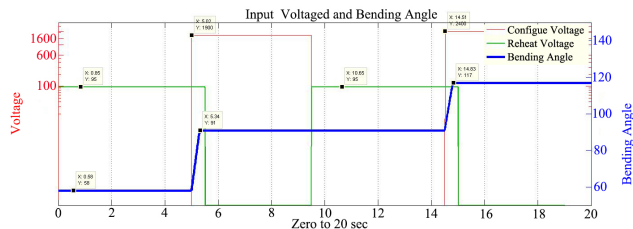


FIGURE 13. Bending angle design (blue line) with the corresponding actuating scheme of reheat voltage (green line) and configure voltage (red line).

the subject’s position, it will return to the detection step. Otherwise, the microcontroller unit (MCU) will control the tubes to align with the person’s position. A cooling/heating area is established, which follows the person’s movements. The details are described below.

B. ACTUATING ALGORITHM DESIGN

The control algorithm is based on the parameters of the BSEP material. We need to use two kinds of power to control the panel. One of them is the preheating power, for which we use 95 V/10 mA to preheat and soften the panel. Then, a high voltage is used to configure and activate the panel to change its bending angle. Figure 11 shows the relationship between the bending angle and applied voltage. At 0 V, the initial angle

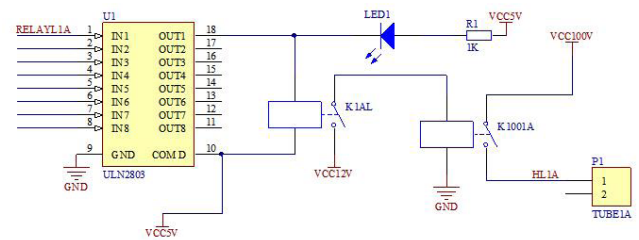


FIGURE 14. Part of actuating circuit.

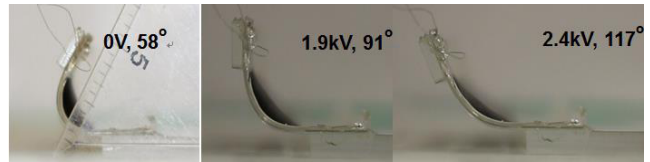


FIGURE 15. Material bending for different actuating voltages.

is 58°. At 2.4 kV, the bending angle of the panel actuator can reach 117°. To carry out a diffusing angle modification, we need to soften the material for 5.5 s and then allow 4 s for it to stabilize. For example, if we want to change the panel’s bending angle from 58° to 91° and then to 117°, we need to configure the power, as shown in Fig. 13. If we want to change the bending angle of a tube, we only need to change the configured voltage.

C. HARDWARE DESIGN AND VALIDATION TEST

To power the panel BSEP actuators (16 for a complete register), a 12-V DC voltage is converted by a DC/DC converter to a voltage between 0 and 3 kV, which can be controlled by a DC control signal. We need to use a high voltage to preheat and configure the tubes. A normal relay would not be able to handle such a high voltage directly. At the same time, a high-power relay cannot use a voltage in the order of 3.3 V to actuate its switch. Considering this situation, we designed a multi-stage output control circuit, using one normal relay as a front control to switch the 12-V power. Then, we actuated the high-voltage relay using this power. A schematic of the actuating circuit is shown in Fig. 14.

Finally, we designed a case to validate the eSaver control system. We set out to change the panel’s bending angle from 58° to 91° and then to 117°. Timing diagrams for the control voltage and bending angle are shown in Fig. 11. The red line is the configure power, which is used to set the bending angle and to actuate the panel. The green line is the reheat power, which we used to reheat the material and soften the panel. When the power is off, the panel cools, so that the bending angle remains fixed. The blue line shows the bending angle under the effect of the control voltage. Figure 15 shows the bending of the material with the configured voltage sequence.

V. CONCLUSION

This paper has presented a novel HVAC system that is capable of achieving significant energy savings in building air-conditioning. A smart register modulates the airflow from a duct to simultaneously provide a high-speed air curtain

to surround an individual occupant, and low-speed inner air within the curtain. First, we demonstrated that this airflow pattern could reduce the overall energy cost by up to 30% relative to the conventional method, and that it could guarantee occupant comfort.

The design of the register features funnel-shaped tunnels, which prove that it could achieve the desired airflow patterns. Moreover, according to CFD simulations, the air volume and velocity from the register could be modified while it was operating by changing the tunnels' dimensions, and could be tailored to suit the thermal needs of various occupants. To enable efficient design optimization, a high abstraction model was developed to predict the diffused airflow from the register. The model was validated as having an error not exceeding 10%, and was found to be 1000 times more efficient than the detailed CFD simulations.

Finally, a prototype of the eSaver was implemented based on an EAP capable of electrically induced large-strain deformation. Thus, adjustments of the register's tunnels could be achieved, and a prototype with the corresponding actuating circuit design was demonstrated.

This work focused on the prototyping of the overall system, although much of the system-level optimization remains to be done in the future. The conditioning effect and comfort level are highly related to the register's dimensions and the size of the holes, so we will research the latter in our future research. The set-points for the conditioning air volume, temperature, and diffusing angle will also be optimized to realize greater savings.

REFERENCES

- [1] K. Wang et al., "A survey on energy Internet: Architecture, approach, and emerging technologies," *IEEE Syst. J.*, to be published, doi: 10.1109/JSYST.2016.2639820.
- [2] H. Jiang, K. Wang, Y. Wang, M. Gao, and Y. Zhang, "Energy big data: A survey," *IEEE Access*, vol. 4, pp. 3844–3861, Aug. 2016.
- [3] K. Wang, Z. Ouyang, R. Krishnan, L. Shu, and L. He, "A game theory-based energy management system using price elasticity for smart grids," *IEEE Trans. Ind. Informat.*, vol. 11, no. 6, pp. 1607–1616, Dec. 2015.
- [4] (Mar. 2014). *Estimation Base on Energy Information Administration's (EIA) Annual Energy Overview*. [Online]. Available: <http://www.eia.gov/forecasts/aeo/er/retrieved>
- [5] A. Rabl and A. Rialhe, "Energy signature models for commercial buildings: Test with measured data and interpretation," *Energy Buildings*, vol. 19, no. 2, pp. 143–154, Aug. 1992.
- [6] E. A. Arens, F. S. Bauman, L. P. Johnston, and H. Zhang, "Testing of localized ventilation systems in a new controlled environment chamber," *Indoor Air*, vol. 1, no. 3, pp. 263–281, Sep. 1991.
- [7] B. Yang, "Thermal comfort and indoor air quality evaluation of a ceiling mounted personalized ventilation system integrated with an ambient mixing ventilation system," Ph.D. dissertation, Dept. of Building, Nat. Univ. Singapore, Singapore, 2009.
- [8] B. Yang, C. Sekhar, and A. K. Melikov, "Ceiling mounted personalized ventilation system in hot and humid climate—An energy analysis," *Energy Buildings*, vol. 42, no. 12, pp. 2304–2308, Dec. 2010.
- [9] L. J. Lo and A. Novoselac, "Localized air-conditioning with occupancy control in an open office," *Energy Buildings*, vol. 42, no. 7, pp. 1120–1128, Jul. 2010.
- [10] A. Makhoul, K. Ghali, and N. Ghaddar, "Ceiling-mounted fresh air personalized ventilator system for occupant-controlled microenvironment," in *Proc. ASME Int. Mech. Eng. Congr. Expo.*, Nov. 2012, pp. 1683–1693.
- [11] ASHRAE Research. (2009). *ASHRAE handbook—Fundamentals*. Amer. Soc. Heating, Refrigerating and Air-Conditioning Eng., Atlanta, GA, USA.
- [12] A. R. Haftkhani and M. Arabi, "Improve regression-based models for prediction of internal-bond strength of particleboard using Buckingham's pi-theorem," *J. Forestry Res.*, vol. 24, no. 4, pp. 735–740, Dec. 2013.
- [13] M. Robnik-Šikonja and I. Kononenko, "Theoretical and empirical analysis of ReliefF and RReliefF," *Mach. Learn.*, vol. 53, nos. 1–2, pp. 23–69, Oct. 2003.
- [14] Y. Lei and H. Liu, "Feature selection for high-dimensional data: A fast correlation-based filter solution," in *Proc. 20th Int. Conf. Mach. Learn. (ICML)*, Washington, DC, USA, 2003, pp. 856–863.
- [15] R. Kohavi and G. H. John, "Wrappers for feature subset selection," *Artif. Intell.*, vol. 97, nos. 1–2, pp. 273–324, 1997.
- [16] A. R. Conn, N. I. M. Gould, and P. L. Toint, *Trust Region Methods*. Philadelphia, PA, USA: SIAM, Aug. 2000.
- [17] B. A. Boukamp, "A nonlinear least squares fit procedure for analysis of immittance data of electrochemical systems," *Solid State Ionics*, vol. 20, no. 1, pp. 31–44, Feb. 1986.
- [18] R. Pelrine, R. Kornbluh, Q. Pei, and J. Joseph, "High-speed electrically actuated elastomers with strain greater than 100%," *Science*, vol. 281, no. 5454, pp. 836–839, Feb. 2000.
- [19] F. Carpi et al., "Standards for dielectric elastomer transducers," *Smart Mater. Struct.*, vol. 24, no. 10, p. 105025, Sep. 2015.
- [20] Z. Ren, W. Hu, C. Liu, S. Li, X. Niu, and Q. Pei, "Phase-changing bistable electroactive polymer exhibiting sharp rigid-to-rubbery transition," *Macromolecules*, vol. 49, no. 1, pp. 134–140, Dec. 2015.

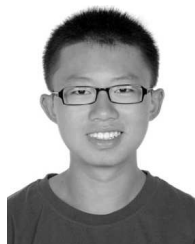


JINLONG YAN was born in Bengbu, China, in 1988. He received the M.S. degree in microelectronics from Anhui University, Hefei, China, in 2014, where he is currently pursuing the Ph.D. degree in microelectronics.

From 2014 to 2016, he was a Research Assistant with the Electronic Engineering Department, University of California at Los Angeles, Los Angeles, CA, USA. His research interests include the development of embedded systems, deep learning, and

the Internet of Things.

Mr. Yan received the Chinese Government Scholarship for study abroad, the National Scholarship, and the China (International) Transducer and Sensor Innovation Contest. He holds four patents during his study years.



QI ZENG is currently pursuing the bachelor's degree in electrical engineering from Tsinghua University, Beijing, China. He was a full-time Visiting Researcher with Prof. He's IoT Group, University of California at Los Angeles, Los Angeles, CA, USA, in 2016.

He is currently an undergraduate Research Assistant in two national key labs on power systems with Tsinghua University, focusing on systems analysis, data science, mathematical optimization, and game theory.

He placed second in the 2015 Npower Forecasting Challenge, U.K., and in the 2016 BigDEAL Forecasting Competition, USA.



YUAN LIANG was born in Tianjin, China. He received the bachelor's degree in automation from Zhejiang University, China, in 2015. He is currently pursuing the Ph.D. degree in electrical engineering with University of California at Los Angeles (UCLA), Los Angeles, CA, USA.

In 2013, he was an undergraduate Research Assistant with the Electronic and Computer Engineering Department, Hong Kong University of Science and Technology, Hong Kong. In 2014, he was a summer intern Research Assistant with the Electrical Engineering Department, UCLA. His research interests include the Internet of Things and deep learning.

Mr. Liang received the National Scholarship by the Chinese Government.



LEI HE received the Ph.D. degree in computer science from the University of California at Los Angeles (UCLA), Los Angeles, CA, USA, in 1999.

Since 2010, he has been a Full Professor with the Electronic Engineering department, University of California at Los Angeles. From 2006 to 2010, he was an Associate Professor with the Electronic Engineering Department, UCLA. His research interests include VLSI circuits and sys-

tems, cyber-physical systems and Internet-of-Everything systems for smart grids, electric vehicles, energy and water conservation, and health care.

Dr. He is the Founding Director of the UCLA Global Clean Energy Research Center (CERC-LA, <http://cerc.ucla.edu>). He received the IEEE design automation conference (DAC) Top-10 Author Award for the Fifth Decade from 2004 to 2013 and the IEEE Design Automation Conference Prolific Author Award, DAC 25 Club, in 2013.



ZHENGPING LI was born in Xuan Cheng, China, in 1979. He received the Ph.D. degree in physical electronics from the University of Science and Technology of China, Hefei, China, in 2004.

Since 2004, he has been an Associate Professor with the School of Electronics and Information Engineering, Anhui University, China. From 2014 to 2015, he was a Senior Visiting Scholar with the Electronic Engineering Department, University of California at Los Angeles,

Los Angeles, CA, USA. His research interests include embedded systems, machine learning, and integrated circuits.

Dr. Li is the Vice President of the Instrument Institute of Anhui Province. He received the Anhui Province Science and Technology Progress Prize twice.

...